

Femtosecond laser user facility for application research onultrafast science

Zhaohua Wang(王兆华), Shaobo Fang(方少波), Hao Teng(滕浩), Hainian Han(韩海年), Xinkui He(贺新奎), Zhiyi Wei(魏志义)

Citation: Chin. Phys. B . 2018, 27(7): 074202. **doi:** 10.1088/1674-1056/27/7/074202

Journal homepage: http://cpb.iphy.ac.cn; http://iopscience.iop.org/cpb

What follows is a list of articles you may be interested in

A tunable XUV monochromatic light source based on the time preserving grating selection of high-order harmonic generation

Yong Niu(牛永), Hongjing Liang(梁红静), Yi Liu(刘燚), Fangyuan Liu(刘方圆), Ri Ma(马日), Dajun Ding(丁大军)
Chin. Phys. B . 2017, 26(7): 074222. **doi:** 10.1088/1674-1056/26/7/074222

Generation of femtosecond laser pulses at 263 nm by $K_3B_6O_{10}Cl$ crystal

Ning-Hua Zhang(张宁华), Shao-Bo Fang(方少波), Peng He(何鹏), Hang-Dong Huang(黄杭东), Jiang-Feng Zhu(朱江峰), Wen-Long Tian(田文龙), Hong-Ping Wu(吴红萍), Shi-Lie Pan(潘世烈), Hao Teng(滕浩), Zhi-Yi Wei(魏志义)
Chin. Phys. B . 2017, 26(6): 064208. **doi:** 10.1088/1674-1056/26/6/064208

High-energy femtosecond Yb-doped all-fiber monolithic chirped-pulse amplifier at repetition rate of 1 MHz

Zhi-Guo Lv(吕志国), Hao Teng(滕浩), Li-Na Wang(王立娜), Jun-Li Wang(王军利), Zhi-Yi Wei(魏志义)
Chin. Phys. B . 2016, 25(9): 094208. **doi:** 10.1088/1674-1056/25/9/094208

19-fs pulse generated by supercontinuum compression

Hua-Qiang Zhang(张华强), Peng Wang(王鹏), Wen-Jun Liu(刘文军), Yi-Lei Yao(姚翳蕾), Zhi-Jing Xu(徐志敬), Jian Li(李健)
Chin. Phys. B . 2016, 25(2): 024209. **doi:** 10.1088/1674-1056/25/2/024209

Frequency doubled femtosecond Ti:sapphire laser with an assisted enhancement cavity

Jin-Wei Zhang(张金伟), Hai-Nian Han(韩海年), Lei Hou(侯磊), Long Zhang(张龙),Zi-Jiao Yu(于子蛟), De-Hua Li(李德华), Zhi-Yi Wei(魏志义)
Chin. Phys. B . 2016, 25(1): 014205. **doi:** 10.1088/1674-1056/25/1/014205

Super-resolution imaging via sparsity constraint and sparse speckle illumination*

Pengwei Wang(王鹏威)[1,2], Wei Li(李伟)[2,3], Chenglong Wang(王成龙)[1,2], Zunwang Bo(薄遵望)[1], and Wenlin Gong(龚文林)[1,†]

[1] *Key Laboratory for Quantum Optics and Center for Cold Atom Physics, Shanghai Institute of Optics and Fine Mechanics, Chinese Academy of Sciences, Shanghai* 201800, *China*

[2] *University of Chinese Academy of Sciences, Beijing* 100049, *China*

[3] *Academy of Opto-electronics, Chinese Academy of Sciences, Beijing* 100094, *China*

(Received 5 February 2018; revised manuscript received 19 March 2018; published online 25 June 2018)

We present an imaging approach via sparsity constraint and sparse speckle illumination which can dramatically enhance the optical system's imaging resolution. When the object is illuminated by some sparse speckles and the sparse reconstruction algorithm is utilized to restore the blur image, numerical simulated results demonstrate that the image, whose resolution exceeds the Rayleigh limit, can be stably reconstructed even if the detection signal-to-noise ratio (SNR) is less than 10 dB. Factors affecting the quality of the reconstructed image, such as the coded pattern's sparsity and the detection SNR, are also studied.

Keywords: imaging and optical processing

PACS: 42.30.–d

DOI: 10.1088/1674-1056/27/7/074202

1. Introduction

Images with high spatial resolution are always required in most imaging applications especially in life science, material science, and remote sensing. For conventional imaging, the optical system's imaging resolution is restricted by the imaging system's Rayleigh limit and the camera's pixel resolution.[1] A series of methods are proposed to break the optical system's Rayleigh limit, which is often called super-resolution imaging. Generally speaking, super-resolution reconstruction approaches can be divided into two cases. One is single-frame super-resolution reconstruction, and the other is multi-frame super-resolution reconstruction.[2] For single-frame super-resolution reconstruction, the light intensity distribution illuminating the object is usually uniform, and some prior information like sparsity and probability density is utilized.[2–7] For multi-frame super-resolution reconstruction, the light intensity distribution on the object for each frame may be uniform or heterogeneous. For the former, the imaging resolution is enhanced because the object's high-frequency can be obtained by looking at the same object from different angles.[8] For the latter, super-resolution imaging can be obtained based on the random and sparsity property of the speckle illuminating the object. Examples include the ghost imaging,[9,10] fluorescence imaging,[11,12] and structured illumination microscopy.[13–15] However, the improvement of imaging resolution for the super-resolution reconstruction approaches described above is limited in practice because of the effect of detection noise or the complexity of the object.[16–18] Therefore, it is natural to ask whether some robust super-resolution imaging methods can be developed by adopting the mutual advantages of present super-resolution reconstruction techniques. For example, the sparse reconstruction algorithm has a great advantage to obtain super-resolution images of sparse objects.[3–5] If the object is not sparse, we can use some sparse speckle patterns to illuminate the object, then each image transmitted/reflected from the object becomes sparse and super-resolution reconstruction of complex objects can also be realized by the sparse reconstruction algorithm. Also, high-order correlated imaging can improve the system's imaging resolution to some extent,[19] which is possible to further improve the imaging resolution of super-resolution imaging via sparse speckle illumination.

In this paper, by combining the advantage of sparse speckle illumination with the characteristic of high-order correlated imaging, a super-resolution imaging approach via sparsity constraint and sparse speckle illumination is proposed. We have demonstrated by numerical simulation the super-resolution ability of the proposed approach. The influences of the coded pattern's sparsity at the object plane and the detection signal-to-noise ratio (SNR) to the reconstruction quality are also discussed.

2. Model of the proposed approach

A typical optical imaging system, as shown in Fig. 1(a), usually consists of an illumination source, an object, an imaging component, and a detector. When the illumination light is

*Project supported by the National Natural Science Foundation of China (Grant No. 61571427).

†Corresponding author. E-mail: gongwl@siom.ac.cn

© 2018 Chinese Physical Society and IOP Publishing Ltd

fully spatially incoherent, the intensity at the detection plane is the convolution of the intensity transmitted from the object with the incoherent point spread function (PSF)[16]

$$I_{\rm im}(x,y) = [S(x,y)\cdot I_{\rm obj}(x,y)] \otimes h(x,y) + n(x,y), \quad (1)$$

where $\otimes$ denotes the convolution operation, $S(x,y)$ is the intensity distribution of the light field illuminating the object, $h(x,y)$ is the optical imaging system's PSF, $n(x,y) = 10^{-\beta}\max\{[S(x,y)\cdot I_{\rm obj}(x,y)] \otimes h(x,y)\}G(x,y)$ (the entries of $G(x,y)$ satisfy a Gaussian distribution with mean 0 and variance 1) denotes the detection noise, and the detection SNR is 10β. In addition, $I_{\rm obj}(x,y)$ is the object's transmission function, and $I_{\rm im}(x,y)$ is the image intensity.

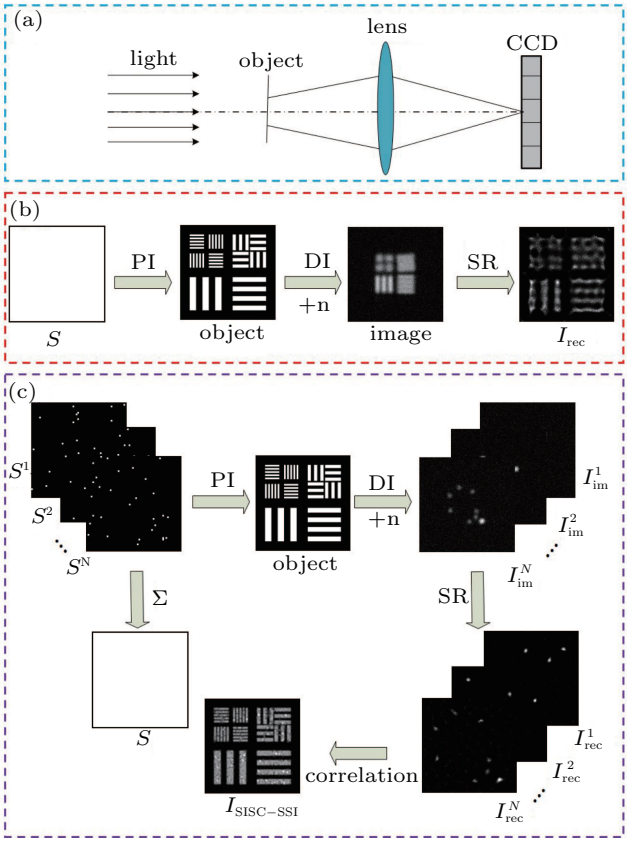


Fig. 1. (color online) (a) The schematic of a typical optical imaging system. (b) Single-frame super-resolution reconstruction via uniform illumination. (c) Procedure of super-resolution imaging via sparsity constraint and spare speckle illumination. CCD: charge-coupled device; PI: projection illumination; DI: diffraction-limited; SR: sparse reconstruction; S^1–S^N are the random sparse speckle patterns; and $\sum$ denotes the summation.

For the schematic of single-frame super-resolution reconstruction shown in Fig. 1(b), $S(x,y)$ is uniform and we have implemented the Lucy–Richardson algorithm in the image reconstruction process.[20,21] The reconstruction algorithm is based on the Bayesian analysis and the assumption that each image's pixel follows the Poisson distribution. Then the original target is reconstructed by maximizing the posterior probability according to the blur image and the system's PSF. The optimization process can be expressed as

$$I_{\rm rec}(x,y) = I^s_{\rm obj}(x,y); \quad \text{which maximizes}$$

$$\prod_{x,y} \frac{[I^s_{\rm obj}(x,y)\otimes h(x,y)]^{I_{\rm im}(x,y)}\, {\rm e}^{-I^s_{\rm obj}(x,y)\otimes h(x,y)}}{I_{\rm im}(x,y)!}, \quad (2)$$

where $I_{\rm rec}(x,y)$ is the reconstruction result.

For the proposed method of super-resolution imaging via sparse speckle illumination depicted in Fig. 1(c), a series of random sparse speckle patterns $S^1(x,y)$–$S^N(x,y)$ illuminate the same object in turn. Because the optical system is diffraction-limited, we can obtain a sequence of blur images $I^1_{\rm im}(x,y) - I^N_{\rm im}(x,y)$ correspondingly, namely,

$$\begin{aligned} I^i_{\rm im}(x,y) &= [S^i(x,y)I_{\rm obj}(x,y)] \otimes h(x,y) + n(x,y) \\ &= I^i_{\rm obj}(x,y) \otimes h(x,y) + n(x,y), \quad (3) \\ S(x,y) &= \sum_{i=1}^{N} S^i(x,y), \quad (4) \end{aligned}$$

where $S^i(x,y)$ and $I^i_{\rm obj}(x,y) = S^i(x,y)I_{\rm obj}(x,y)$ are the intensity distribution of the sparse speckle pattern illuminating the object and the image transmitted from the object in the i-th frame, respectively. In addition, N is the total frame number and $S(x,y)$ is the total intensity distribution of the sparse speckle patterns at the object plane. In order to guarantee the gray fidelity of the reconstructed image, $S(x,y)$ is usually set to be homogeneous and there is no speckles' overlap between any two frames. Therefore, the speckle area $a\times a$, the total frame number N, the speckle's number K (the number of bright spots per frame), and the reconstruction area $L\times L$ satisfy the relation $L\times L = N\times K\times a\times a$.

According to each blur image $I^i_{\rm im}(x,y), i = 1,\ldots,N$, we can obtain corresponding $I^i_{\rm rec}(x,y)$ by the reconstruction algorithm of Eq. (2). For multi-frame imaging via speckle illumination, high-order correlated imaging can improve the system's imaging resolution to some extent compared with the traditional directly integral imaging,[19] hence the final image is also reconstructed by calculating the high-order correlation function of the light field, which is called as super-resolution imaging via sparsity constraint and sparse speckle illumination (SISC-SSI), namely,

$$I_{\rm SISC-SSI}(x,y) = \left\{\frac{1}{N}\sum_{i=1}^{N}(I^i_{\rm rec}(x,y) - \langle I^i_{\rm rec}(x,y)\rangle)^2\right\}^{1/2}, \quad (5)$$

where $\langle I^i_{\rm rec}(x,y)\rangle = \frac{1}{N}\sum_{i=1}^{N} I^i_{\rm rec}(x,y)$ represents the ensemble average of $I^i_{\rm rec}(x,y)$.

In summary, the reconstruction procedure of SISC-SSI can be expressed as the following three steps:

1) Obtain a sequence of blur images $I^1_{\rm im}(x,y)$–$I^N_{\rm im}(x,y)$ by Eq. (3).

2) Reconstruct $I^i_{\rm rec}(x,y)$ by Eq. (2) according to $I^i_{\rm im}(x,y)$ and PSF.

3) Obtain the final image $I_{\rm SISC-SSI}(x,y)$ by Eq. (5).

3. Simulation results and discussion

Figure 2 presents the principle schematic of SISC-SSI. The uniform and incoherent light emitted from a xenon lamp is collimated by a lens with a focal length of f_0 and then filtered by an optical filter (with a center wavelength of $\lambda = 532$ nm). The light transmitted from the filter propagates to a digital micro-mirror device (DMD). A series of coded patterns, as shown in Fig. 1(c), are pre-built by modulating the DMD and then imaged onto the object by the lens with the focal length $f_1 = 75$ mm. The light transmitted from the object is imaged onto a charge-coupled device (CCD) camera by a $4f$ optical system. An Iris with the diameter D is placed at the focal plane of the lens $f = 250$ mm, which is used to control the system's diffraction limit. In the simulation experiment, the resolution test chart (Fig. 3(a)) is utilized as the object, the object is composed of four sets of different slit widths (120×120 pixels, the pixel size is 3.45 μm × 3.45 μm). The object's center-to-center separation is $d_1 : d_2 : d_3 : d_4 = 1 : 2 : 3 : 4$ and $d_1 = 13.8$ μm. The image recorded by the CCD camera has 240×240 pixels and the pixel size of the CCD camera is also 3.45 μm ×3.45 μm. In addition, the coded region on the DMD is 60×60 pixels and the pixel size of the DMD is 13.68 μm × 13.68 μm. In order to match the speckle's transverse size at the object plane with the pixel size of the CCD camera, the distances z_1 and z_2 are set as 223.7 mm and 112.8 mm, respectively, which means that the speckle's transverse size illuminating on the object is 6.9 μm.

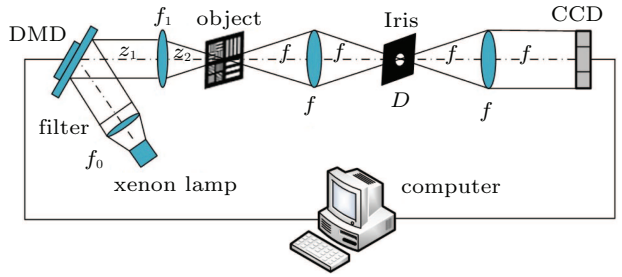


Fig. 2. (color online) Schematic of super-resolution imaging via sparsity constraint and sparse speckle illumination.

Under a uniform illumination, we can adjust the Iris's transmission aperture to make some details of the target undistinguished (the spatial resolution is about $d_3 = 41.4$ μm). In this case, the transverse size of the Iris is approximately $D \approx 1.22\lambda f/d_3 = 3.9$ mm and the optical system's PSF is displayed in Figs. 3(a_2) and 3(a_3). Correspondingly, the blur image of the object in different detection SNR is illustrated in Figs. 3(b_1)–3(b_5). Based on Eq. (2), when the detection area on the CCD camera is chosen as 240×240 pixels and 120×120 pixels, figures 3(c_1)–3(c_5) and 3(d_1)–3(d_5) give the corresponding single-frame reconstruction results, respectively. It is clearly seen that the object's image can be restored without noise when the detection area is twice as large as the object area (Fig. 3(c_1)), whereas single-frame reconstruction is disabled even if the detection SNR reaches 20 dB (Fig. 3(c_2)). In contrast with Figs. 3(c_1)–3(c_5), when the detection area is the same as the object area (the area labeled by the red rectangular box in Figs. 3(b_1)–3(b_5), the object can not be restored even without noise (Figs. 3(d_1)–3(d_5)). Correspondingly, when the object is illuminated by some random sparse speckle and the detection area is the same as the object area, figures 3(e_1)–3(e_5) present one frame of detection image in different detection SNR and the corresponding recovered results based on Eq. (2) are shown in Figs. 3(f_1)–3(f_5). When the speckle number is 5 in each frame, the reconstruction results of SISC-SSI are displayed in Figs. 3(g_1)–3(g_5). It is obvious that SISC-SSI can stably reconstruct the object and robust to noise. Therefore, we have demonstrated the validity of our super-resolution approach and the imaging resolution can be smaller than the diffraction limit by $1/3$.

In Fig. 4, we show the simulated SISC-SSI reconstruction results of imaging the same object displayed in Fig. 3(a) when the coded pattern's sparsity (the speckle's number at the object plane) is different and the detection SNR is 10 dB. In Fig. 4(a), each illumination has only one speckle, which is the same as point scanning imaging[22] and has the best reconstruction quality because each image restored is the sparsest.[3,4,9] However, the measurement number N is the largest. From Figs. 4(a)–4(f), we can find that as the speckle's number illuminating the object is increased, the reconstruction resolution will decay.

In order to evaluate quantitatively the influence of the speckle's number and detection SNR to the reconstructed results of SISC-SSI, the reconstruction quality is estimated by calculating the peak signal-to-noise ratio (PSNR)

$$\mathrm{PSNR} = 10 \times \log_{10}\left[\frac{(2^p-1)^2}{\mathrm{MSE}}\right], \tag{6}$$

where the bigger the PSNR is, the better the quality of the recovered image is. For a 0–255 gray-scale image, $p = 8$ and MSE represents the mean square error of the reconstruction image $I_{\mathrm{SISC-SSI}}$ with respect to the original object I_{obj}

$$\mathrm{MSE} = \frac{1}{N_{\mathrm{pix}}}\sum\nolimits_{x,y}\left[I_{\mathrm{SISC-SSI}}(x,y) - I_{\mathrm{obj}}(x,y)\right]^2. \tag{7}$$

Here N_{pix} is the total pixel number of the image. From Fig. 5, it is obviously seen that the PSNR always increases with the detection SNR and decreases with the speckle's number at the object plane, which is also consistent with the results indicated in Figs. 3 and 4.

To validate the applicability of SISC-SSI for more general images, we give a numerical experimental demonstration of imaging a continuous varying gray-scale object, i.e., a slide representing a detail of the picture "lena" (120×120

pixels). Figures 6(b_1)–6(b_5) illustrate SISC-SSI results in different detection SNR and the reconstructed results with different speckle's numbers are shown in Figs. 6(c_1)–6(c_5), which are similar to the results shown in Figs. 3(g_1)–3(g_5) and 4(a)–4(f). Therefore, we further demonstrate the feasibility of the SISC-SSI approach for practical applications.

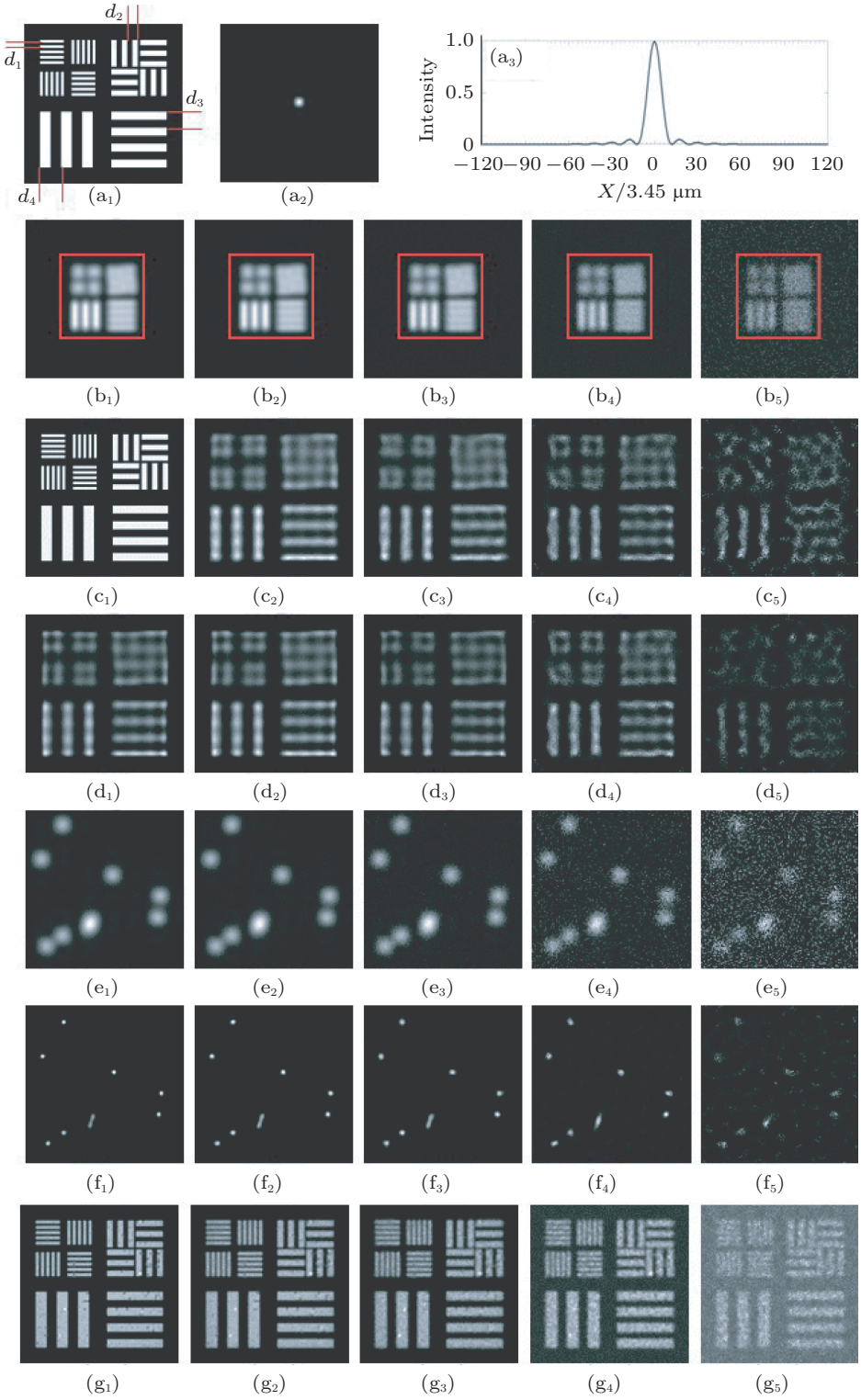


Fig. 3. (color online) (a_1) Original object. (a_2) The PSF corresponding to a spatial resolution of 41.4 μm. (a_3) Cross section of PSF along ($x, y = 0$) of (a_2). (b_1)–(b_5) The images recorded by the CCD camera in different detection SNR (the image area labeled by the red rectangular box is 120×120 pixels). (c_1)–(c_5) Single-frame reconstruction results via uniform illumination (the detection area recorded by the CCD camera is 240×240 pixels). (d_1)–(d_5) Single-frame reconstruction results via uniform illumination based on the detection data shown in the red rectangular box. (e_1)–(e_5) One frame of detection image in different detection SNR for SISC-SSI. (f_1)–(f_5) The reconstruction results corresponding to the images of (e_1)–(e_5). (g_1)–(g_5) The reconstruction results of SISC-SSI in different detection SNR when the speckle's number is 5 for each frame. From left to right, the detection SNR is ∞, 20 dB, 15 dB, 10 dB, and 5 dB, respectively.

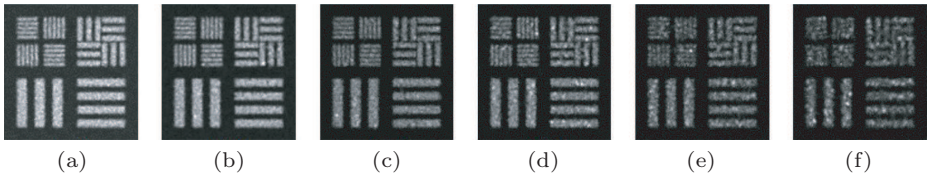


Fig. 4. (color online) The influence of the speckle's number illuminating on the object to SISC-SSI when the detection SNR is 10 dB for each frame. The speckle's number is 1, 5, 15, 30, 60, and 120 for (a)–(f), which is corresponding to $N = 3600$, 720, 240, 120, 60, and 30, respectively.

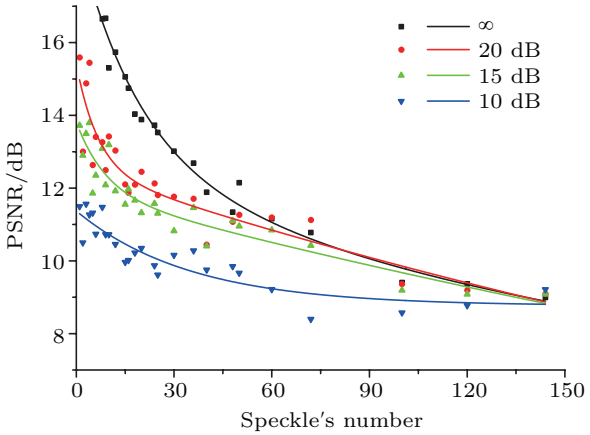


Fig. 5. (color online) The relationship between PSNR and the speckle's number in different detection SNR.

Generally speaking, similar to super-resolution imaging via sparsity constraint,[3–5,9] the object's sparsity is mainly utilized by the method of SISC-SSI. By random sparse speckle illumination, a complex target is divided into many sparse objects so that the sparse reconstruction algorithm is valid to super-resolution reconstruction. Compared with point scanning imaging (the result shown in Figs. 4(a) and 6(c_1)), like spinning disk confocal and multi-focal structured illumination microscopy,[14,22] although the imaging quality is degraded slightly as the speckle's number is properly increased (Figs. 4(b)–4(f) and 6(c_2)–6(c_5)), the measurement number N can be dramatically decreased. Our reconstruction method has utilized the object's sparsity and the imaging resolution depends on the sparse degree of objects (namely, the speckle number per frame), which is different from point scanning imaging. Searching for better reconstruction algorithm is the main direction of further improvement of our method. What is more, some ideas of SISC-SSI may be adopted by ghost imaging to further improve the imaging resolution, such as sparse speckle illumination and multiple-input detection, which will be our next work.

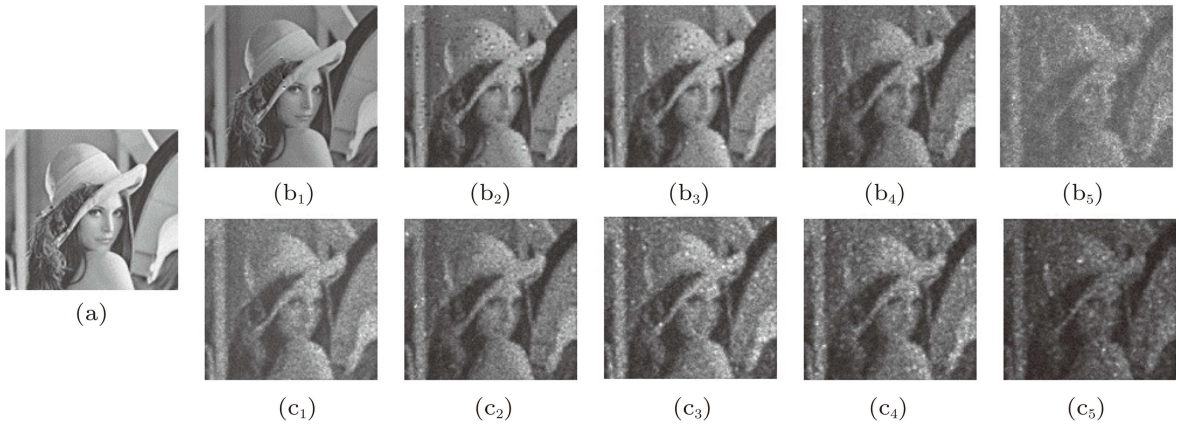


Fig. 6. (color online) Numerical experimental demonstration of SISC-SSI for a gray-scale object. (a) Original object. (b_1)–(b_5) The results of SISC-SSI in the detection SNR = ∞, 20 dB, 15 dB, 10 dB, and 5 dB, respectively, and the speckle's number is 5. (c_1)–(c_5) The results of SISC-SSI when the speckle's number is 1, 5, 10, 15, and 30, respectively, and the detection SNR is 10 dB.

4. Conclusion

We demonstrate the reconstruction of images borne on sparse speckle illumination and sparsity constraint at a resolution greatly exceeding the finest resolution defined by the optical system's diffraction limit. We also show that the method of super-resolution imaging is robust to noise and the coded pattern's sparsity has an obvious influence on the reconstruction quality. This technique will be useful to microscopy in biology, material, and medical sciences.

References

[1] Rayleigh L 1879 *Philos. Mag.* **5** 261
[2] Park S C, Park M K and Kang M G 2003 *IEEE Signal Process Mag.* **20** 21
[3] Szameit A, Segev M, Gazit S and Eldar Y C 2009 *Opt. Express* **17** 23920
[4] Shechtman Y, Gazit S, Szameit A, Eldar Y C and Segev M 2010 *Opt. Lett.* **35** 1148

[5] Xue C B, Yao X R, Li L Z, Li X F, Yu W K, Guo X Y, Zhai G J and Zhao Q 2017 *Chin. Phys. B* **26** 024203
[6] Yang J, Wright J, Huang T S and Ma Y 2010 *IEEE Trans. Image Process.* **19** 2861
[7] Schulz R R and Stevenson R L 1996 *IEEE Trans. Image Process.* **5** 996
[8] Elad M and Feuer A 1997 *IEEE Trans. Image Process.* **6** 1646
[9] Gong W L and Han S S 2015 *Sci. Rep.* **5** 9280
[10] Gong W L 2015 *Photon. Res.* **3** 234
[11] Hell S W and Wichmann J 1994 *Opt. Lett.* **19** 780
[12] Rust M J, Bates M and Zhuang X 2010 *Nat. Methods* **3** 793
[13] Mudry E, Belkebir K, Girard J, Savatier J, Moal E L, Nicoletti C, Allain M and Sentenac A 2012 *Nat. Photon.* **6** 312
[14] York A G, Parekh S H, Nogare D D, Fischer R S, Temprine K, Mione M, Chitnis A B, Combs C A and Shroff H 2012 *Nat. Methods* **9** 749
[15] Min J, Jang J, Keum D, Ryu S W, Choi C, Jeong K H and Ye J 2013 *Sci. Rep.* 2075
[16] Goodman J W 1968 *Introduction to Fourier Optics* (New York: McGraw-Hill)
[17] Hunt B R 1995 *Int. J. Imaging Syst. Technol.* **6** 297
[18] Kolobov M I 2007 *Quantum Imaging* (New York: Springer) Chap. 6
[19] Zhang P, GongW, Shen X, Huang D and Han S 2009 *Opt. Lett.* **34** 1222
[20] Lucy L B 1974 *Astron. J.* **79** 745
[21] Richardson and William H 1972 *J. Opt. Soc. Am.* **62** 55
[22] Zhao G Y, Zheng C, Fang Y, Kuang C F and Liu X 2017 *Acta Phys. Sin.* **66** 148702